PHYSICAL REVIEW B **80**, 140412(R) (2009)

Quantum magnetoelectric effect in iron garnet

Yuichi Yamasaki,[1] Yuki Kohara,[1] and Yoshinori Tokura[1,2,3]
[1]*Department of Applied Physics, University of Tokyo, Tokyo 113-8656, Japan*
[2]*Multiferroics Project, ERATO, Japan Science and Technology Agency, Tokyo 113-8656, Japan*
[3]*Cross-Correlated Materials Research Group (CMRG), RIKEN, Wako 351-0198, Japan*
(Received 2 October 2009; published 27 October 2009)

The magnetoelectric response and its quantum relaxation phenomenon have been investigated for a single crystal of yttrium iron garnet. The electric-dipole moments, built in by excess localized electrons forming Fe^{2+} sites, never freeze even at the lowest temperature and relax through a quantum tunneling process. Application of magnetic field enhances the dielectric relaxation strength and gives rise to a large magnetocapacitance effect ($\sim$13% at 10 K with 0.5 T). We show that this magnetically tunable quantum paraelectricity is associated with the Fe^{2+}-based magnetoelectric centers in which the electric polarization depends on the magnetization vector via the spin-orbit coupling.

DOI: 10.1103/PhysRevB.80.140412 PACS number(s): 75.80.+q, 71.70.Ej, 75.50.Gg, 77.22.Gm

There has been growing interest in dynamical coupling between electric and magnetic-dipole moments, which may lead to the dynamical control of electric polarization (magnetization) in terms of temporally varying magnetic (electric) field. One such example is the terahertz electrically driven magnetic resonance or the so-called electromagnon[1–3] and another is the electrically driven motion of the magnetic domain walls;[4] both have recently been observed in a family of multiferroics with coexistent ferroelectric and magnetic orders. Another important category of such a dynamical magnetoelectric coupling is the magnetocapacitance (MC) effect in which the external magnetic field changes the ac dielectric response. In principle, any insulator with spin degree of freedom is allowed to show more or less such a MC effect, for example, via the lattice effect on the spin-exchange interaction (exchange striction mechanism). Nevertheless, realization of the gigantic MC effect with a small external magnetic field is highly nontrivial and such giant-MC materials are still very rare.[5,6,8,9] Here, we report on the finding of the large MC effect in one of the most orthodox insulating ferromagnets, yttrium iron garnet $Y_3Fe_5O_{12}$ (YIG), as characterized by magnetically tunable (both in field magnitude and direction) quantum paraelectricity. The underlying physics is unique but may find many other applications; the electric-dipole can be hosted by the impuritylike Fe^{2+} site where the spin-orbit interaction governs the quantum-mechanical relaxation process in response to the external magnetic field or the magnetization vector.

A family of iron garnet has been extensively studied because of their widespread technological applications, e.g., microwave devices and magneto-optical isolators.[10] The unit cell of YIG crystal is composed of three tetrahedron (FeO_4) and two octahedron (FeO_6) iron-oxygen clusters. The Fe spins in these two clusters are antiferromagnetically coupled with each other, yielding a ferrimagnetic order below $T_c \sim 550$ K with the magnetic easy axis along the four $\langle 111 \rangle$ directions. It has been known for long that YIG and related compounds show the second-order magnetoelectric effect.[11,12] Although the magnetic-group theoretical analyses provided some understanding of the phenomena,[13] the microscopic mechanism remains to be clarified. The E-induced ME effect is equivalent to the MC effect due to the relation that $\alpha_{ME}=(\partial\varepsilon/\partial H)E$ (Ref. 1); therefore, the full understanding of the MC effect may provide a key to solve the puzzling origin of ME effect for YIG.

Single crystals of YIG or Ca-doped analogs were grown using a traveling-solvent floating zone method in oxygen gas flow.[14] The crystal was oriented using Laue x-ray diffraction pattern and cut into thin plate with the widest faces perpendicular to the [001] axis. Dielectric constants were measured using an LCR meter (Agilent E4980A) and impedance analyzers (Solartron 1260, 1296) with an applied ac electric field $E_{ac}\|[001]=4$ kV/m at frequencies of $1 \leq f \leq 10^6$ Hz.

Figure 1 shows the dependence of real part of dielectric constant (ε') measured with 10 Hz electric field (E) along [001] on the magnetic fields ($H\|$[001], [010], and [110]), together with the corresponding M-H curves. M starts to saturate at a relatively low field ($<$0.3 T) with the common saturation $M(\sim 5.2\mu_B/\text{f.u.})$ for all H directions. The ε' increases concomitantly with the magnetic domain rotation and becomes constant with saturated M. The observed MC effect depends remarkably on the direction of M and monotonously increases as temperature decrease [Figs. 1(b) and 1(c)]. The maximum value of MC ratio $[\Delta\varepsilon/\varepsilon(0\ \text{T})]$ exceeds 10% for $H\|$[001], which is fairly large as compared with those previously reported in dielectric ferromagnets.[6–9] This kind of anisotropic MC effect resembles that of $Tb_3Fe_5O_{12}$ and Mn_3O_4, where the anisotropic (such as tetragonal or orthorhombic) lattice-structural domain can be aligned with application of H through a magnetostriction effect. However, this mechanism is readily ruled out for the present case because the saturated M is isotropic along all crystallographic axes and the magnetostriction constant in YIG [$\lambda \sim 8\times 10^{-6}$ (Ref. 15)] is 2 orders of magnitude smaller than in those materials [e.g., $\lambda \sim 10^{-3}$ in $Tb_3Fe_5O_{12}$ (Ref. 8)].

To clarify the origin of the observed MC effect, we have investigated the dielectric relaxation (DR) and magnetic relaxation (MR) phenomenon. Figure 2 shows the evolution of the real (ε') and imaginary (ε'') part of the dielectric dispersion with varying temperature (T) at 0 T [Figs. 2(a) and 2(b)] and at 0.5 T [Figs. 2(c) and 2(d)] for the applied $H\|$[001] in which the largest MC effect is observable. The dielectric dispersion curves are described by the Havriliak-Negami relaxation model,[16] $\varepsilon=\varepsilon_\infty+\Delta\chi/(1+(i\omega\tau)^\alpha)^\beta$, which is an em-

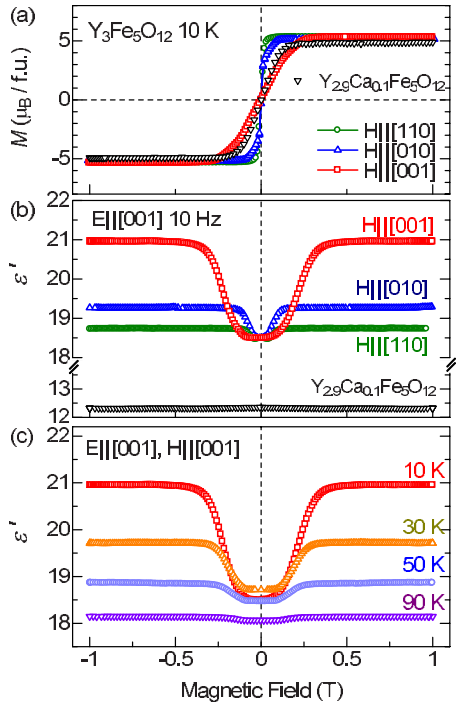

FIG. 1. (Color online) Magnetic field dependence of (a) magnetization (M), (b) real part of dielectric constant (ε'), and (c) ε' for $H\|[001]$ at several temperatures for $Y_3Fe_5O_{12}$ in the comparison with poly crystal $Y_{2.9}Ca_{0.1}Fe_5O_{12}$. The difference in M between $H\|[001]$ and [010] is caused by a demagnetization effect due to the sample shape.

pirical modification of the Debye relaxation model ($\alpha=\beta=1$) with a relaxation strength $\Delta\chi$ and relaxation time τ. The exponents α and β stand for the asymmetry and broadness of the dispersion, respectively, and vary within ranges of $0.65<\alpha<1$ and $0.6<\beta<0.95$ in the present (H,T) region.

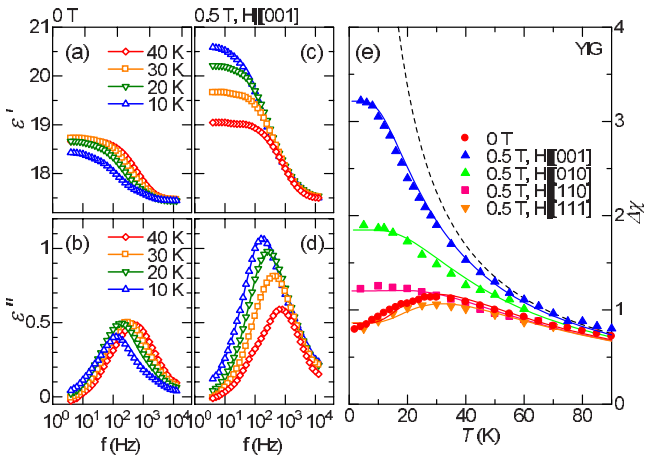

FIG. 2. (Color online) Temperature dependence of real part dielectric constants ε' (a) and (b) and imaginary part ε'' (c) and (d). (e) Temperature dependence of relaxation strength $\Delta\chi$ for 0 T and for four different directions of H ([001], [010], [110], and [111]). The obtained fitting parameters Ω and Γ for the transverse-field Ising model (see text) are 42 and 50 K for 0 T, 42 and 0 K for $H\|[001]$, 73 and 0 K for $H\|[010]$, 73 and 42 K for $H\|[110]$, and 52 and 54 K for $H\|[111]$, respectively.

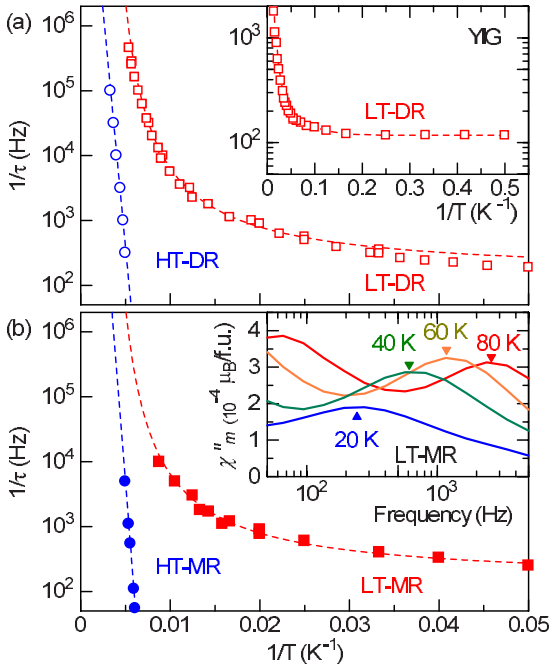

FIG. 3. (Color online) Inverse temperature dependence of (a) high-temperature and low-temperature dielectric relaxations (HT-DR and LT-DR) and (b) magnetic relaxation rates (HT-MR and LT-MR). The broken lines are the guide to the eyes. The inset of (a) covers a lower-T region, and the inset of (b) shows the evolution of LT-MR in the imaginary part of magnetic susceptibility (χ''_m).

The distinct DRs can be observed down to 2 K, in which τ appears almost T independent at low T and $\Delta\chi$ displays a clear difference in magnitude between 0 and 0.5 T. These behaviors indicate that the MC effect originates from the H-induced variation of $\Delta\chi$. Figure 2(e) shows the T dependence of $\Delta\chi$ at 0 T and at H applied along various crystallographic directions. The $\Delta\chi$ for $H\|[001]$ increases monotonically down to 10 K and becomes almost constant below 10 K. Similar behaviors are also observed for $H\|[010]$ and $H\|[110]$. On the other hand, for zero field and $H\|[111]$ (magnetic easy axis), $\Delta\chi$ shows a broad maximum at around 30 K and gently decreases with further lowering T. The deviation from the classical Curie law [$\Delta\chi\propto T^{-1}$ as indicated by a broken line in Fig. 2(e)] is reminiscent of quantum paraelectricity.[20,21]

For the analysis of the relaxation dynamics we show the Arrhenius plot for the dielectric and magnetic relaxation rate (τ^{-1}) versus the inverse temperature (T^{-1}) in Fig. 3. Besides the low-temperature DR (LT-DR) as depicted in Fig. 2, the high-temperature DR (HT-DR) shows up above 100 K and its relaxation strength is a few orders of magnitude larger than LT-DR. In accord with the DRs, some MRs are observed to emerge in the magnetic susceptibility χ_m; here we show the high-temperature and low-temperature magnetic relaxations (HT-MR and LT-MR) in Fig. 3(b).[17] The high-temperature relaxations can be described by the Arrhenius law, $\tau^{-1}\propto\exp(-E_a/k_BT)$ with the Boltzmann constant k_B, an attempt frequency f_0 and an activation energy E_a. The HT-DR and HT-MR show, respectively, $E_a=0.29$ and 0.34 eV, which are both ascribed to the polaron hopping

process.[18,19] As decreasing temperature, these HT-DR and HT-MR rapidly freeze up while the LT-DR and LT-MR subsist and show large deviations from the Arrhenius law at low temperatures; the LT-DR rate tends to be independent of T below 10 K and remains finite ($\tau^{-1} \sim 100$ Hz) even at the lowest temperature. Moreover, the temperature variations of relaxation rates of LT-DR and LT-MR almost coincide, signaling that these DR and MR share the origin; i.e., they are *magnetoelectric* in nature.

To analyze the $\Delta\chi(T,H)$ data showing the quantum relaxation behavior, we have considered a simple two-level model.[22] The essence can be captured by (noninteracting) transverse-field Ising model, $\mathcal{H}=-\Omega\Sigma_i S_i^x-\Gamma\Sigma_i S_i^z$, where S_i^α denotes a pseudospin operator representing the electric-dipole moment state at ith site and Ω a transverse field representing quantum-mechanical tunneling. Here Γ corresponds to a longitudinal field, $\Gamma=\Delta E+2\vec{\mu}\cdot\vec{E}$; the first term is for an energy splitting ΔE between the pseudospin (dipole moment $\vec{\mu}$) up and down level and the second term for the coupling of the dipole moment to an electric field $\vec{E}$. The thermal expectation value of the pseudospin is

$$\langle\vec{S}\rangle = \frac{1}{2}\frac{\vec{F}}{|\vec{F}|}\tanh\left(\frac{|\vec{F}|}{2k_BT}\right), \tag{1}$$

with an effective field $\vec{F}=(\Omega,0,\Gamma)$. The static polarization P and the dielectric susceptibility $\Delta\chi$ are calculated such as $P=2n\mu\langle S^z\rangle$ and $\varepsilon_0\Delta\chi=(\partial P/\partial E)_{E=0}$. Here, n denotes the number of dipoles per unit volume and $\mu=|\vec{\mu}|$. The best fitting of the $\Delta\chi(T)$ curves gives the parameters; $n\mu^2/\varepsilon_0=135$ K, Ω ranging from 42 to 73 K, and Γ ranging from 0 to 54 K (see the caption of Fig. 2).

Here, we consider the origin of the MC effect and the relaxations. As shown in Fig. 1, the large MC effect as observed in YIG is totally negated in Ca-doped YIG ($Y_{3-x}Ca_xFe_5O_{12}$),[23] which is equivalent to carrier-electron compensated YIG. The result implies that the emergence of MC effect requires excess electrons, which may be donated by the oxygen vacancies. Such an excess electron moving between the two (or more) equivalent potential wells would give rise to the dielectric relaxation.[24,25] Furthermore, the magnetically anisotropic $Fe^{2+}(3d^6)$ ion formed by the excess electron, causes the magnetic relaxation, as observed.[19]

The Fe^{2+}-states are expected to occupy the octahedron sites rather than the tetrahedron sites.[19,26,27] In the FeO_6 octahedron, the oxygen cage is trigonally distorted with D_{3h} symmetry; therefore, their symmetry axis coincides with one of the four different $\langle 111\rangle$ axes [see Fig. 4(a)]. There are at least four equivalent positions of the octahedron, each of which has its symmetry axis along the respective $\langle 111\rangle$. The trigonal crystal field splits the t_{2g} manifold into singlet (a_{1g}) and doublet (e_g). For Fe^{2+}, the doublet is further split due to a spin-orbit coupling ($\lambda\vec{l}\cdot\vec{s}$) between the unquenched angular momentum ($\vec{l}$) pointing to the respective symmetry axes and the spin ($\vec{s}$) [Fig. 4(b)]; thus the energy levels depend on the direction of M. Namely, the application of H can control the longitudinal field Γ through the energy splitting ΔE induced by the spin-orbit coupling and can change the distribution of excess electron from the unpolarized ($\Gamma=0$) to the polarized state ($\Gamma\neq 0$).

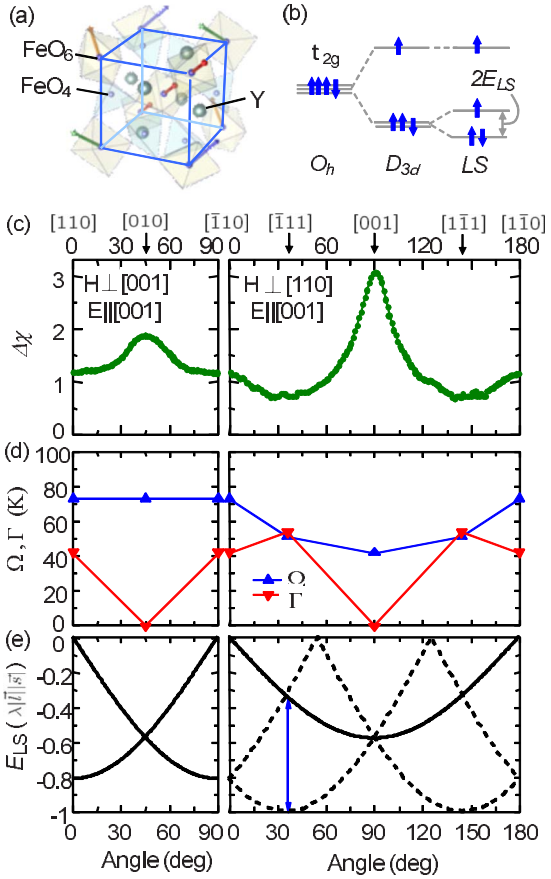

FIG. 4. (Color online) (a) Crystal structure of 1/8 unit cell in YIG. The arrows indicate trigonal symmetry axes in respective octahedron sites. (b) Energy diagram of the $Fe^{2+}(3d^6)t_{2g}$ state on the FeO_6 octahedron site under the trigonal (D_{3h}) crystal field. (c) Dependence of $\Delta\chi$, (d) Γ, and Ω on the orientation of H rotated within the (001) plane (left panel) and the (110) plane (right panel). (e) Energy variation of the spin-orbit coupling ($E_{LS}=\lambda\vec{l}\cdot\vec{s}$) for four different octahedron sites. The solid lines indicate the doubly degenerate states.

To test this hypothesis, we now discuss the H-direction dependence of the MC effect. In spite of the relative small magnetic anisotropy, $\Delta\chi$ shows a clear anisotropic behavior with respect to H; $\Delta\chi$ for $H\|[001]$ is four times as large as that for $H\|[111]$ at 2 K [Fig. 4(c)].[28] In the above model, the application of $H\|[111]$ urges the excess electron to form the Fe^{2+} state on an octahedron site with $\vec{l}\|[111]$. Then, the Fe^{2+} center becomes most polarized with least fluctuation due to a slanted double-well potential, hence $\Delta\chi$ shows the lowest value. Difference of the spin-orbit energy splitting between the octahedron with $\vec{l}\|[111]$ and those with other $\vec{l}(\|\langle 111\rangle)$ directions, as indicated with a vertical arrow in Fig. 4(e), reaches $\Gamma_{LS}=0.67\lambda|\vec{s}||\vec{l}|\sim 78$ K,[19] which is comparable to the observed value $\Gamma=54$ K for $H\|[111]$. On the other hand, the quadruply degenerate state for $H\|[001]$ corresponds to the $\Gamma=0(\Delta E=0)$ state. In this case, the polarizable center shows the maximal fluctuation and shows the quantum paraelectric behavior, leading to the highest value of $\Delta\chi$. The

difference in $\Delta\chi$ between $H\|[010]$ and $H\|[001]$ is ascribable to the difference of Ω [see Fig. 4(d)]. The octahedron sites in YIG crystal are linked by the tetrahedron sites; thus, their states may influence the quantum tunneling Ω. In the case of $H\|\langle 011\rangle$, the nonzero Γ is obtained even though the ground states are doubly, though not quadruply, degenerate. This implies that the dipole moments are constructed not only within the lowest doubly degenerate sites but within more sites, beyond the simple two-level model described above. For further understanding of these magnetoelectric coupling, the microscopic distribution of the polarizable centers in actual YIG crystal should be clarified.

In conclusion, the as-grown crystal of YIG, involving impuritylike oxygen vacancies, was revealed to exhibit the electric-dipole moments with subsisting fluctuation down to the lowest temperature, as characterized by the quantum relaxation. The source of the electric dipole and its fluctuation is likely the excess electron (Fe^{2+}) distribution around the oxygen vacancy and its hopping over the neighboring FeO_6 clusters, which critically depends on the direction of the magnetization (or applied magnetic field) via the spin-orbit interaction of the Fe^{2+} state. This leads to the magnetically tunable quantum paraelectricity as observed at low temperatures below 50 K. The control of quantum dielectric fluctuation with a low magnetic field may add a further variety to magnetoelectric phenomena and find many applications to other magnetic impurity centers endowed with spin-orbit coupling.

We would like to thank N. Oda, H. Murakawa, and F, Kagawa for their help on measurements and Y. Onose, H. Katsura, T. Arima, and N. Furukawa for fruitful discussions. This work was supported in part by Grants-In-Aid for Scientific Research (Grants No. 15104006, No. 17340104, and No. 16076205) from the MEXT of Japan and JSPS.

[1] For special issue of multiferroics, J. Phys.: Condens. Matter **20**, No. 43 (2008).
[2] A. Pimenov, A. A. Mukhin, V. Yu Ivanov, V. D. Travkin, A. M. Balbashov, and A. Loidl, Nat. Phys. **2**, 97 (2006).
[3] N. Kida, Y. Ikebe, Y. Takahashi, J. P. He, Y. Kaneko, Y. Yamasaki, R. Shimano, T. Arima, N. Nagaosa, and Y. Tokura, Phys. Rev. B **78**, 104414 (2008).
[4] F. Kagawa, M. Mochizuki, Y. Onose, H. Murakawa, Y. Kaneko, N. Furukawa, and Y. Tokura, Phys. Rev. Lett. **102**, 057604 (2009).
[5] T. Katsufuji and H. Takagi, Phys. Rev. B **64**, 054415 (2001).
[6] T. Kimura, S. Kawamoto, I. Yamada, M. Azuma, M. Takano, and Y. Tokura, Phys. Rev. B **67**, 180401(R) (2003).
[7] J. Hemberger, P. Lunkenheimer, R. Fichtl, H.-A. Krug von Nidda, V. Tsurkan, and A. Loidl, Nature (London) **434**, 364 (2005).
[8] N. Hur, S. Park, S. Guha, A. Borissov, V. Kiryukhin, and S.-W. Cheong, Appl. Phys. Lett. **87**, 042901 (2005).
[9] T. Suzuki and T. Katsufuji, Phys. Rev. B **77**, 220402(R) (2008).
[10] J. Helszajn, *YIG Resonators and Filters* (John Wiley & Sons, New York, 1985).
[11] T. H. O'Dell, Philos. Mag. **16**, 487 (1967).
[12] H. Ogawa, E. Kita, Y. Mochida, K. Kohn, S. Kimura, A. Tasaki, and K. Siratori, J. Phys. Soc. Jpn. **56**, 452 (1987).
[13] A. J. Freeman and H. Schmid, *Magnetoelectric Interaction Phenomena in Crystals* (Gordon & Breach Science Pub., New York, 1975).
[14] S. Kimura and K. Kitamura, J. Am. Ceram. Soc. **75**, 1440 (1992).
[15] A. E. Clark, H. B. Callen, E. R. Callen, B. Desavage, and W. Coleman, J. Appl. Phys. **34**, 1296 (1963).
[16] S. Havriliak and S. Negami, Polymer **8**, 161 (1967).
[17] We observed another magnetic relaxation in a temperature region between 50 and 120 K; however, it was omitted for simplification.
[18] Y. J. Wu, Y. Gao, and X. M. Chen, Appl. Phys. Lett. **91**, 092912 (2007).
[19] F. Walz, L. Torres, J. Iniguez, and H. Kronmüller, Phys. Status Solidi A **180**, 507 (2000).
[20] K. A. Müller and H. Burkard, Phys. Rev. B **19**, 3593 (1979).
[21] J. H. Barrett, Phys. Rev. **86**, 118 (1952).
[22] J. Hemberger, P. Lunkenheimer, R. Viana, R. Böhmer, and A. Loidl, Phys. Rev. B **52**, 13159 (1995).
[23] Y. Kohara, Y. Yamasaki, and Y. Tokura (unpublished).
[24] I. G. Austin and N. F. Mott, Adv. Phys. **50**, 757 (2001).
[25] V. Narayanamurti and R. O. Pohl, Rev. Mod. Phys. **42**, 201 (1970).
[26] P. K. Larsen and R. Metselaar, Phys. Rev. B **8**, 2016 (1973).
[27] On the basis of the fitting analysis ($n\mu^2/\varepsilon_0 = 135$ K), we can estimate the density (n) of the magnetoelectrically active Fe^{2+} sites; the dipole moment (μ) produced by the electron hopping between the nearest-neighbor octahedron sites is 30 D and hence n is estimated to be 1.7×10^{24} m^{-3} or 2.0×10^{-4}/(octahedron site).
[28] The $\Delta\chi$ curves in Fig. 4(c) were calculated by the difference between ε at 5 and 10^6 Hz as a function of angle.